ORIGINAL PAPER

Mechanical study and molecular dynamics simulation on polycarbonate nanocomposite with carbon black and SnO2

Mehdi Eskandari [1,2] · Jaber Azizi [3] · Rasoul Malekfar [1] · Pablo Taboada [2]

Abstract

In this work, SnO_2 and carbon black (CB) nanoparticles (NPs) were used to improve the physical and mechanical properties of polycarbonate films (PC) for industrial applications. Raman spectroscopy proved the successful inclusion of the fillers within the polymeric-based nanocomposites, with a suitable dispersion without changes in the structure and morphology of PC as denoted by scanning electron microscopy (SEM) and X-ray diffraction (XRD). After doping of the PC-based nanocomposites with CB, SnO_2 and CB/SnO_2 NPs, both the polymer hardness and the elastic modulus of the composites were observed to increase, with the highest value achieved for PC/CB-doped ones. Thermal gravimetric analysis (TGA) and differential scanning calorimetry (DTG) indicated changes in the thermal properties of the polymer composites upon NP doping. Finally, molecular dynamics simulations were used to gain a better understanding about the interactions of PC and NPs in the nanocomposites. Simulation data obtained were in good agreement with experimental ones, which indicates that simulations can be an efficient toll in order to perform a preliminary high-throughput screening of diverse physico-chemical properties of polymeric-based nanocomposites bearing NP fillers before experimental development.

Keywords Polymer-based nanocomposites · Metal oxide · Molecular dynamic simulation · Nanoparticles

Introduction

Recently, polymer nanocomposites have been gained a great deal of interest due to their excellent optical, electrical and mechanical properties [1, 2] in which nanoparticles (NPs) and fillers are used to improve the polymeric matrix´ properties in order to modify existing and/or provide new ones. Polycarbonate (PC) is one of the most used polymers to construct polymeric matrices, thanks to its high level of transparency, toughness and good mechanical strength [3–5]. In addition, PC-based nanocomposites films have not only a good flexibility, but also a good tensile strength which leads to utilize polymer nanocomposites in a wide variety of industrial applications [6–10]. The influence of different NPs and fillers such as graphite, graphene, carbon nanotubes (CNTs), and different types of clays on the thermal [7], mechanical, optical and photochromic properties of PC nanocomposites has been widely analysed. Besides, Carbon Black as a cheap filler has great influence on mechanical properties of nanocomposites, including hardness, Young modulus, tensile strength, tear strength and resistance to abrasion [11–14]. In particular, nanoscale transition metal oxides are particularly appealing for these purposes due to their chemical durability, mechanical stability photocatalytic behavior and surface area. [1] For example, Maniks et al. showed that the addition of $CoFe_2O_4$ NPs led to an improvement of both the hardness and Young's modulus of PC-based nanocomposites. Also, the effect of ZrO_2 and ZnO NPs on the structure, mechanical properties and thermal degradation kinetics have been investigated [15, 16]. Luyt et al. analyzed the effect of nano-SiO_2 which led, in this case, to an enhancement of the thermal and mechanical properties of the developed nanocomposites [17].

✉ Mehdi Eskandari
mehdi.eskandari.phys@gmail.com

✉ Pablo Taboada
pablo.taboada@usc.es

1 Physics Department, Faculty of Basics Sciences, Tarbiat Modares University, Tehran, Iran

2 Colloids and Polymers Physics Group, Condensed Matter Physics Area, Faculty of Physics, Universidade de Santiago de Compostela, A Coruña, Spain

3 Polymer Engineering Department, Tarbiat Modares University, Tehran, Iran

Nonetheless, despite all these ensemble of promising experimental data, the atomistic behavior and interactions between NPs and other fillers and polymeric matrices is still unclear [18]. In this regard, molecular dynamic simulation (MDS) is a powerful tool to attain insights into the nanocomposite features and properties including their thermal and mechanical properties [19–22]. MDS, as a numerical method, solves the motion equations and provide the temporal evolution of the molecular configuration/arrangements, providing the different states of the polymeric based-system [23–25].

In the present work, with the aim of improving in particular the mechanical properties of PC-based nanocomposites, metal oxide SnO_2 and CB NPs were used as fillers and their influence of on the physico-chemical properties of the former polymeric-based nanocomposite was investigated. SnO_2/PC, CB/PC and SnO_2/CB/PC nanocomposites were fabricated in order to determine the physical properties of each type of hybrid system in order to elucidate the potential additive and/or synergistic properties of the dual-modified nanocomposites. To characterize the morphology of the nanocomposite films, scanning electron microscopy (SEM) was used whilst their structure was identified by means of X-ray diffraction (XRD) and Raman spectroscopy. Vickers micro-hardness and tensile tests allowed analyze their mechanical properties. Moreover, thermal gravimetric analysis (TGA) and differential scanning calorimetry (DSC) were used to illustrate the thermal properties of the bare and filler-modified nanocomposites. Finally, the obtained experimental data were used as the initial inputs for molecular dynamic simulations to obtain the simulated nanocomposites mechanical and thermal properties, which were compared with the experimental ones.

Materials and methods

Experimental

Materials

SnO_2 NPs (99.7%) were purchased from Research Nanomaterial, USA. CB was obtained from Simorgh Company (Iran). PC was supplied from Lexan, USA. Dichloromethane (DCM) from Merck (USA) was used as the solvent. All the reagents were used as received without any further purification.

Preparation of nanocomposites

In order to prepare the polymer-based nanocomposites, 1.0 g of PC was dissolved in 10 mL of DCM. Next, SnO_2 NPs (5 wt.%) were dispersed to 10 mL of DCM, then, the former and latter solutions gradually added to the 10 mL DCM while stirring. The final mixed solution was stirred for 5 h. After

mixing, the resulting solution was sonicated by means of an ultrasonic probe (Misonix Sonicator 3000 model S3000MPD, Japon) for 10 min in order to disperse all the NPs in the solution. Afterwards, the solution was stirred again for additional 5 h. Finally, it was poured onto a Petri dish and put in the oven at 30 °C to evaporate the remaining DCM.

The procedure of preparation of the CB/PC nanocomposites was similar as the SnO_2/PC ones. To produce the PC/CB (1 wt.%) /SnO_2 (5 wt.%) nanocomposites, SnO_2/DCM and CB/DCM solutions were prepared separately as previously described. Then, SnO_2/DCM and then CB/DCM solutions were gradually added to a PC/DCM solution. The resulting mixed solution was stirred for 5 h at 750 rpm and, then, probed with an ultrasonic probe for 10 min. Finally, solvent removal was performed as early described. The average thicknesses of the as-prepared films were ca. 200 μm.

Characterization

The crystal structure of the as-obtained polymer nanocomposite films was studied with an X-ray diffractometer (X'pert model 1480, Philips, Netherlands) equipped with a CuKα radiation source. The X-ray wavelength was 1.54056 Å, and the diffraction patterns were recorded at room temperature in a 2θ range of 10 to 70° at a scanning speed of 2°/min. Raman spectroscopy analyses were carried out with an Almega Thermo Nicolet Dispersive Raman spectrometer configured with a microscope (Mplan, Japan) and a TE-cooled silicon charged-coupled device (CCD) array detector. The second harmonic (532 nm) of a Nd:YLF laser was used for excitation. The morphology and microstructure of polymer nanocomposite films were also examined by using a SEM microscope (model XL30, Philips, Netherlands) equipped with a tungsten filament and operated at a voltage of 30 kV. To measure the films hardnesses, a BUEHLER (model 60,044 USA) micro hardness tester was used. Samples were indented with a Vickers diamond pyramid indenter having a square base and a 136° pyramid angle. The hardness was measured by applying a 50 g load at a constant loading time of 30 s. In order to perform the tensile tests, composite film samples were prepared based on the ASTM E8M standard. Tensile testing was done by a SANTAM machine at room temperature under a constant strain rate of 0.001 s^{-1}. The stress-strain curves were calculated based on the results of the force-extension tests. TGA and DSC experiments were performed to analyze the thermal stability of the bare polymeric matrix and nanocomposites. TGA and DSC were simultaneously performed using a Rheometric Scientific Company analyzer apparatus (STA 1500 model, UK). The temperature range studied ranged from room temperature up to 800 °C at a heating rate of 10 °C/min under an argon flow of 70 mL/min.

Simulation procedure

MSD methodology

All simulations were done using Material Studio v6.0 and the Condensed phase Optimized Molecular Potentials for Atomistic Simulation Studies (COMPASS) force-field. The structure of PC, SnO_2 and CB were built using Material Studio libraries. A PC chain containing 30 monomers was built from the repeating unit of tetramethyl bisphenol A. As a consequence of the polymer chain length within the simulation box, the CB morphology was assumed to be similar as a single sheet. Constructed molecules are represented in Fig. 1. A geometry optimization of Forcite modules was used in order to minimize the energy of structures. To build the nanocomposites, amorphous cell moduli were used with the initial cell density set to 1.1 g/cc. To reach the bulk properties, periodic boundary conditions were chosen. Figure 1(a) represents the PC amorphous cell. To calculate the PC and filled-nanocomposites properties Synthia and Forcite modules were used, respectively. Each type of nanocomposites was simulated separately, and the obtained results were compared with the experimental ones.

Geometry optimization in MSD

After building the amorphous cells of nanocomposites, the geometry of the obtained structures was optimized in order to minimize the energy of the systems and to clear out the energy hot spots. This process was done by the geometry optimization task of Forcite modules, and COMPASS was assigned as the force field. A group-based method with a cut-off distance of 18.5 Å was used to calculate the van der Waals energy terms. The electrostatic terms were calculated following the Ewald's method with an accuracy of 10^{-5} kcal/mol. After geometry optimization, 200 PC NPT dynamics with a time step of 1 fs at 298 K at 1 atm was carried out to reach the equilibrium. A nose thermostat and a Berendsen barostat were used to control temperature and pressure,

respectively. At the equilibrium state, the fluctuations of the potential energy, non-bonded energy, and density were low. The energy and density of the system are depicted in Fig. 2 (a) and (b). As shown in these figures, after 200 ps the equilibrium is reached.

Result and discussion

XRD analysis

XRD was performed to decipher the structure of pure PC, PC/SnO_2, PC/CB and PC/SnO_2/CB nanocomposite films. Figure 3 shows the obtained X-ray diffraction patterns. It is observed that upon the addition of SnO_2 NPs to the polymeric PC polymeric films the amorphous character of the polymeric phase decreased. Then, it can be concluded that the crystallinity of SnO_2/PC nanocomposites increased, and these NP may act as nucleation sites for crystal formation. Besides, by adding CB NPs similar results are observed. Finally, the XRD pattern for PC/SnO_2/CB composite is shown in Fig. 3 (d), and a decrease of the amorphous polymeric together with the presence of the diffraction peaks corresponding to SnO_2 NPs can be clearly observed.

Raman spectroscopy

Raman spectroscopy was performed in order to identify the vibrational modes of the different polymeric composites and the extent of inclusion of the NP-based fillers within the films. The 400 to 1700 cm^{-1} regions of the Raman spectra of PC, PC/SnO2, PC/CB and PC/SnO2/CB nanocomposites are shown in Fig. 4 (a) to (d), respectively. The RAMAN spectra is characterized by an intense band at 868 cm^{-1} associated with O–C(O)–O stretching, a set of three bands, 1095 cm^{-1}, 1161 cm^{-1} and 1220 cm^{-1}, due to C–O–C stretching, and bands at 620 and 1587 cm^{-1} corresponding to the phenyl ring stretching modes [26]. Vibrational modes of PC shown in Fig. 4 (a) are in full agreement as those reported in previous works
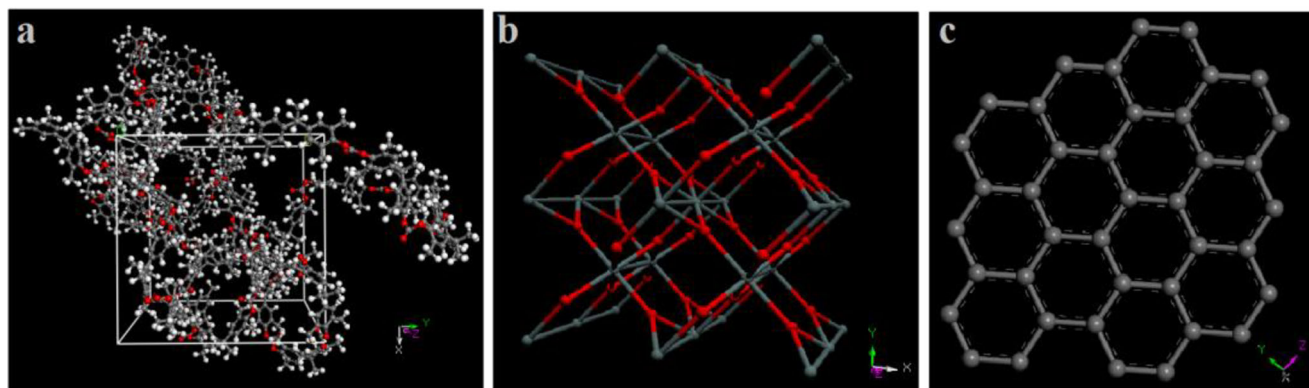

Fig. 1 (a) Molecular model of polycarbonate and typical amorphous cell of polycarbonate; (b) molecular model of SnO_2 and (c) CB NPs
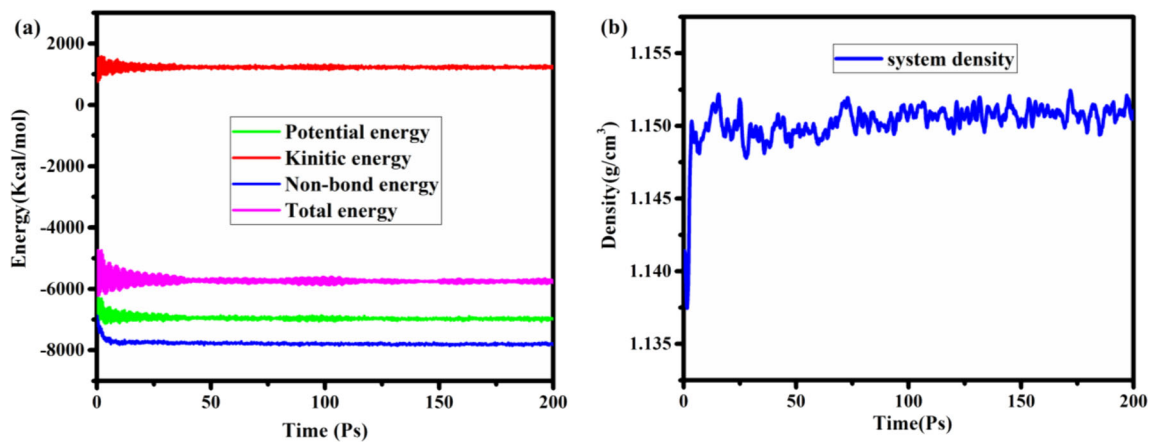
Fig. 2 (*a*). Different contributions to the total energy of the system; (*b*) density of the system.

[27–29]. The Raman spectrum of PC/SnO$_2$ (5 wt.%) is shown in Fig. 4 (b) The recorded spectra illustrate peaks at 473, 632, 696, and 722 cm^{-1} in agreement with previously reported studies [30]. Two peaks at 632 and 692 cm^{-1} be related to the vibrating mode of Sn–O bonds which vibrate in the plane perpendicular to the c-axis. Besides, 473 cm^{-1} mode may be related to the vibration of oxygen in the oxygen plane which vibrates in the direction of the c-axis. For PC/CB (1 wt.%) films (see Fig. 4(c)), the peaks observed at 1385 and 1600 cm^{-1} can be assigned to CB which are related to D and G bands respectively [31]. The latter observed vibration can

be overlapped with the bond stretching of quaternary carbons of the polycarbonate polymer. For PC/SnO$_2$/CB nanocomposites peaks corresponding to CB increase its intensity as a consequence of an overlapping with those stemming from SnO$_2$ NPs vibrations.
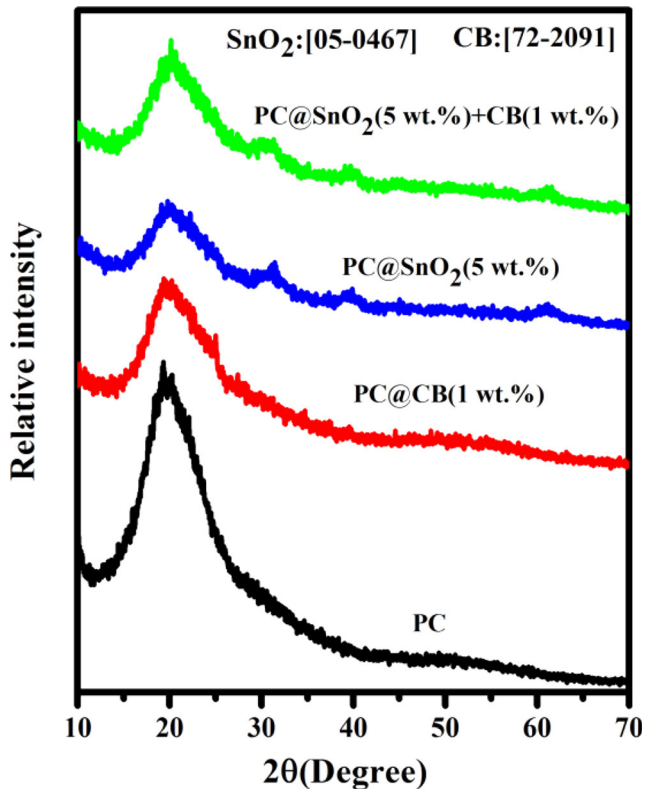

Fig. 3 XRD patterns of (a) PC; (b) PC/SnO$_2$; (c) PC/CB; and (d) PC/SnO$_2$/CB nanocomposites
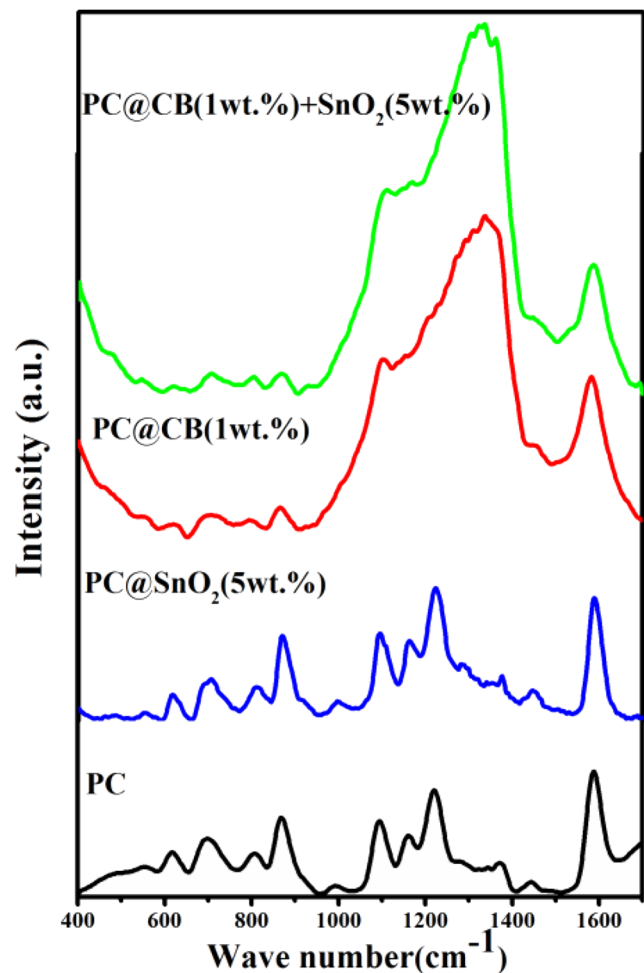

Fig. 4 Raman spectra of (a) PC (b) PC/SnO$_2$ (c) PC/CB (d) PC/SnO$_2$/CB nanocomposites

Tensile tests

Mechanical analysis is a technical analysis used to determine and characterize the mechanical and elastic properties of polymeric-based materials. The stress-strain curves of PC, PC/SnO$_2$, PC/CB and PC/SnO$_2$/CB nanocomposite films are illustrated in Fig. 5. It is possible to observe a certain increase in the stress peaks corresponding to PC/NP composites compared to the bare PC one as a consequence of an enhancement of cohesion between the polymeric chains and the added NPs. As observed, stress profiles denote a very fast increase until a maximum at low applied strains, followed by a subtle decrease and a more continuous increment as the strain is increased. The presence of the observed peak can be correlated to the development of a de-cohesion between the filled NPs and polymeric chains. After the observed peak, plastic deformation was developed. It is also clearly noted that the added NPs have a great influence on the mechanical strength of the PC matrix. Particularly, CB improves the strength of PC in comparison with SnO$_2$ and SnO$_2$/CB. As shown in Fig the elastic properties of PC with CB nanoparticles improved more in comparison with SnO2/CB nanoparticles.

On the other hand, a tensile assay was used to obtain the elastic modulus of the films as a function of the type of added NP (see Fig. 6). Almost all the polymers are visco-elastic materials, and their behavior under a time-dependent creep or stress relaxation is more relevant in comparison with tensile testing. Mostly, the latter is often used to determine the elastic modulus (E) as a function of other variables. Figure 6 shows the variation of E with SnO$_2$, CB, and SnO$_2$/CB NPs within the polymeric films. By adding 5% wt of SnO$_2$, the elastic modulus increased by about 8%. The remarkable improvement of the elastic
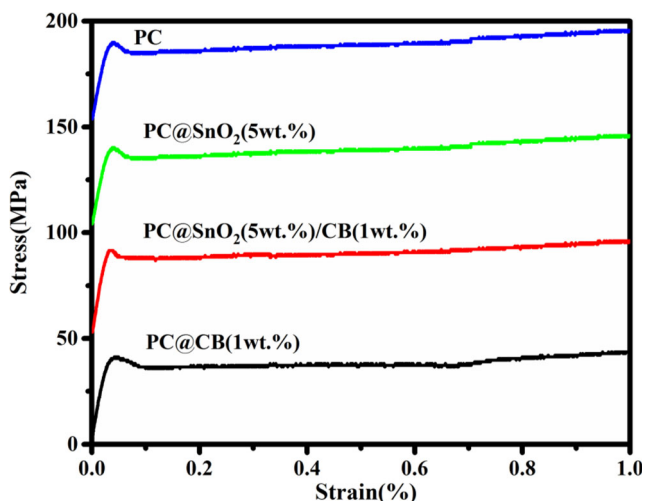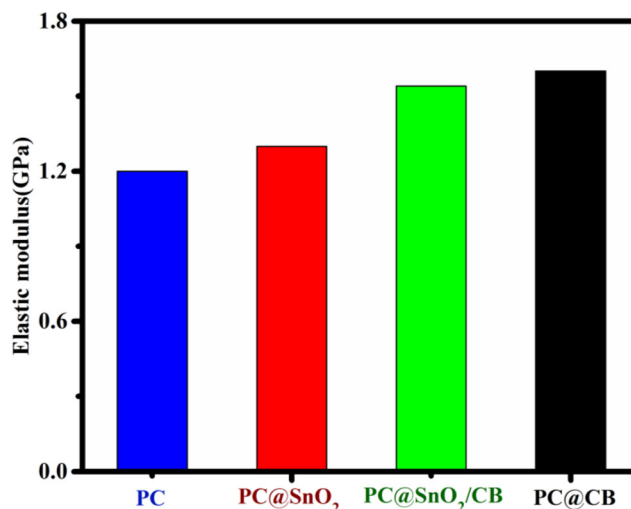

Fig. 6 Elastic modulus of PC, PC/SnO$_2$, PC/CB and PC/SnO$_2$/CB nanocomposites

modulus observed when CB and SnO$_2$ were added to PC. In addition, greater values of Young's modulus were measured for adding CB which is simply attributed to the partly or completely immobilization of PC polymeric chains due to the interaction with CB nanoparticles.

Hardness

Micro hardness values obtained for PC, PC/SnO$_2$ (5 wt.%), PC/CB (1 wt.%) and PC/SnO$_2$/CB nanocoposite films were 11.5, 13.5, 16.1 and 15.4 Vickers, respectively, in agreement with the derived moduli values from tensile test experiments. It is observed that the PC matrix stiffness improves by adding the NP-based fillers, especially for CB possibly due to the large interactions/miscibility between CB NPs and the PC matrix.

TGA

TGA analysis is a popular technique to analyze the thermal stability of polymeric systems under certain conditions in which changes in the sample mass are monitored upon temperature variations. Figure 7 (a) and (b) show TGA and DSC curves for pure PC, PC/CB, PC/SnO$_2$ and PC/SnO$_2$/CB nanocomposites. The degradation of the samples is observed from these figures, in which the SnO$_2$ and SnO$_2$/CB nanocomposites displayed a lower degradation in comparison with the pure PC film, whilst the PC/CB composite shows the highest thermal resistance in comparison with the SnO$_2$ and SnO$_2$/CB-filled ones, highlighting again the strong bonding between CB and PC chains.

Fig. 5 Stress-strain curves for PC, PC/SnO$_2$, PC/CB and PC/SnO$_2$/CB nanomposites
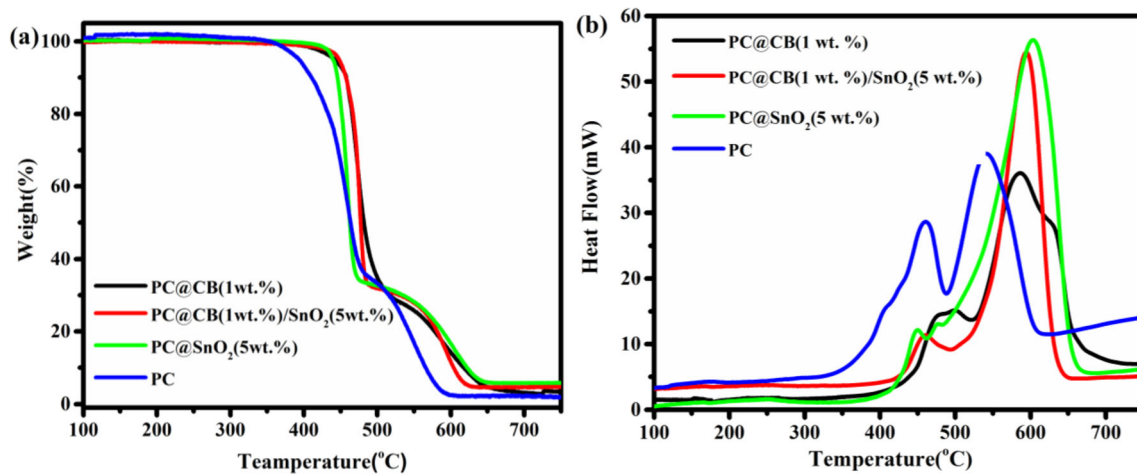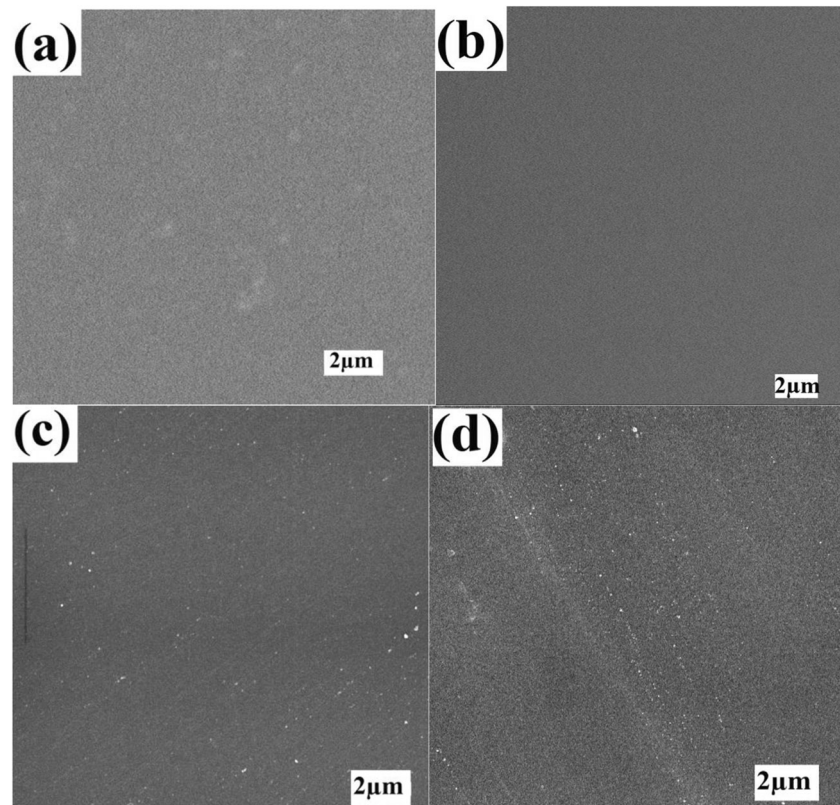
Fig.7 (a) TGA curves for pure PC, PC/CB, PC/SnO₂ and PC/SnO₂/CB nanocomposites, (b) DTG curves for pure PC, PC/CB, PC/SnO₂ and PC/SnO₂/CB nanocomposites

SEM

In Fig. 8 (a) to (d), SEM images of the different nano-composites are shown. It is observed that a thin layer of PC covers the added NPs, with a uniform distribution of these inside the polymeric matrix. From the images an uniform distribution of the NPs within the polymeric films acan be also confirmed, particularly, for the PC/CB composite.

Simulations

Firstly, several properties of pure PC composites with different polymer molecular weight (M_w) were calculated (see Table 1). Based on the simulation results, PC3 with a M_w of 11,000 g/mol has a T_g of ca. 443 K in agreement with previous results (experimental T_g has been set at ca. 423 K), and as the polymer M_w increases T_g also does, as also occur for the bulk, shear and Young's moduli [32].

Fig. 8 SEM images of a) PC b) PC/CB c) PC/SnO2 d) PC/SnO₂/CB nanocomposites (scale bars are 2 μm)

Table 1   Simulation and experimental results of different properties of polycarbonate with different molecular weight

properties	PC1	PC2	PC3	PC4	PC5	PC5	Experimental data [33]
Molecular weight	5000	8000	11,000	14,000	17,000	20,000	11,000
Glass transition temperature Tg (K)	413.2	434.2	443.8	449.3	452.8	455.3	423
Glass transition temperature Tg for infinite molecular weight (k)	469.3	469.3	469.3	469.3	469.3	469.3	–
Density at 298 K (g/cm^3)	1.08	1.08	1.08	1.08	1.08	1.08	1.2
Cohesive energy (Fedors) at 298 K	109.29	109.29	109.29	109.29	109.29	109.29	–
Solubility parameter (Fedors) at 298 K	19.50	19.50	19.50	19.50	19.50	19.50	–
Surface tension (Fedors) at 298 K (mN/m)	39.36	39.36	39.36	39.36	39.36	39.36	42.9
Thermal conductivity at 298 K (W/mK)	0.174	0.174	0.174	0.174	0.174	0.174	0.192
Bulk modulus (GPa)	3.56	3.67	3.71	3.74	3.75	3.76	–
Shear modulus (MPa)	964	992	1000	1010	1020	1020	–
Young's modulus (GPa)	2.650	2.730	2.760	2.780	2.790	2.800	2.38
Poisson's ratio at 298 K	0.376	0.376	0.376	0.376	0.376	0.376	–
Shear yield stress (MPa)	74.2	76.4	77.4	77.9	78.3	78.5	62.1
Brittle fracture stress for infinite molecular weight (MPa)	68.8	68.8	68.8	68.8	68.8	68.8	–

Other physical properties such as density, cohesive energy, solubility and thermal conductivity (all obtained at 298 K) were constant and independent of the polymer M_w. By looking at the calculated values it can be concluded that simulations allow a good estimation of the physical properties of PC films with accuracy.

Next, the estimation of some of the physical properties of NP-filled PC nanocomposites was obtained by MSD using the Forcite modulus. Table 2 displays the simulation results, which are in fair agreement with those obtained experimentally. As can be seen in Table 2 and fig. 8, the software has been more successful in calculating the raw polycarbonate modulus, and with the addition of nanoparticles to the system, the difference in simulation and laboratory values has slightly increased. This difference appears to be due to the complexity of computing the interaction of molecules in the presence of nanoparticles, since in raw polymer only the interaction of polymer-polymer molecules is implied, but by adding nanoparticles, particle-particle and polymer-particle interactions, is added to the calculations.

Conclusions

Here, PC-based nanocomposites filled with two different types of NPs, SnO$_2$ and CB, were prepared. XRD data showed that the addition of the fillers to the PC films enhances the crystallinty. Besides, a uniform distribution of the filled NPs along the polymeric films could be confirmed. Moreover, the mechanical properties of bare PC and NP-filled PC-based nanocomposites revealed that their hardness is increased after the addition of the NPs, especially for CB ones. The use of NPs within the polymeric substrates also improved their thermal properties. The combination of the polymeric film and CB inside (1 wt.% (resulted in the formation of nanocomposite with the largest elastic modulus, hardness and thermal stability. Using molecular dynamics simulations, different physical properties of the developed nanocomposites were calculated and the obtained results indicate a suitable agreement with the experimental data, thus, can be concluded that MSD can be a powerful tool for predicting and perming high-throughput screening of the physical properties of polymer-based nanocomposites.

Table 2   simulation results of PC and PC nanocomposites

	Young Modulus (GPa)	Poisson ratios			Bulk modulus (GPa)			Shear modulus (GPa)			Lame constants (GPa)		Cohesive energy density (J/m^3)	Solubility parameter (J/cm^3)$^{0.5}$
		Exy	Eyx	Ezx	Reuss	Voigt	Hill	Reuss	Voigt	Hill	Lambda	Mu		
PC	1.44	0.435	0.351	0.336	2.53	1.00	1.77	0.767	0.595	0.681	1.5882	0.35	2.536e+008	15.9
PC/SnO$_2$	1.57	0.320	0.412	0.40	2.794	3.00	2.898	0.725	0.968	0.846	1.943	1.071	2.551751e+008	16.1
PC/CB	2.33	0.548	0.477	0.162	2.163	2.47	2.319	0.599	0.932	0.766	2.168	0.853	2.443953e+008	15.6
PC/CB/SnO$_2$	2.29	0.668	0.732	0.286	1.834	2.607	2.220	0.903	1.230	1.066	1.293	1.353	2.647445e+008	16.2

References

1. Eskandari M, Najafi Liavali M, Malekfar R, Taboada P (2020) Investigation of Optical Properties of Polycarbonate/TiO2/ZnO Nanocomposite: Experimental and DFT Calculations. J Inorg Organomet Polym. https://doi.org/10.1007/s10904-020-01644-0

2. Wen T, Guo Y, Song S, Sun S, Zhang H (2015) Inhibited transesterification on the properties of reactive core-shell particles toughened poly(butylene terephthalate) and polycarbonate blends. J Polym Res 22:1–10. https://doi.org/10.1007/s10965-015-0869-1

3. Bao D, Liao X, He T, Yang Q, Li G (2013) Preparation of nanocellular foams from polycarbonate/poly(lactic acid) blend by using supercritical carbon dioxide. J Polym Res 20. https://doi.org/10.1007/s10965-013-0290-6

4. Jiang L, Zhou M, Ding Y, Zhou Y, Dan Y (2018) Aging induced ductile-brittle-ductile transition in bisphenol a polycarbonate. J Polym Res 25:1–9. https://doi.org/10.1007/s10965-018-1443-4

5. Sako T, Ito A, Yamaguchi M (2017) Surface segregation during injection molding of polycarbonate/poly (methyl methacrylate) blend. J Polym Res 24:2–6. https://doi.org/10.1007/s10965-017-1251-2

6. Ongaro M, Signoretto M, Trevisan V, Stortini A, Ugo P (2015) Arrays of TiO2 nanowires as Photoelectrochemical sensors for hydrazine detection. Chemosensors 3:146–156. https://doi.org/10.3390/chemosensors3020146

7. Jaleh B, Shahbazi N, Jabbari A (2016) Optical and thermal properties of polycarbonate-TiO2 Nanocomposite film. Synth React Inorg Met Nano-Metal Chem 46:602–607. https://doi.org/10.1080/15533174.2014.988821

8. Arlinghaus FJ (1974) Energy bands in stannic oxide (SnO2). J Phys Chem Solids 35:931–935. https://doi.org/10.1016/S0022-3697(74)80102-2

9. Yuliarto B, Gumilar G, Septiani NLW (2015) SnO2 nanostructure as pollutant gas sensors: synthesis, sensing performances, and mechanism. Adv Mater Sci Eng 2015:1–14. https://doi.org/10.1155/2015/694823

10. Jubault M, Pulpytel J, Cachet H, Boufendi L, Arefi-Khonsari F (2007) Deposition of SnO2:F thin films on polycarbonate substrates by PECVD for antifouling properties. Plasma Process Polym 4:330–335. https://doi.org/10.1002/ppap.200730903

11. Ramesan MT (2005) The effects of filler content on cure and mechanical properties of dichlorocarbene modified styrene butadiene rubber/carbon black composites. J Polym Res 11:333–340. https://doi.org/10.1007/s10965-005-6571-y

12. Nootsuwan N, Wattanathana W, Jongrungruangchok S, Veranitisagul C, Koonsaeng N, Laobuthee A (2018) Development of novel hybrid materials from polylactic acid and nano-silver coated carbon black with distinct antimicrobial and electrical properties. J Polym Res:25. https://doi.org/10.1007/s10965-018-1484-8

13. Song J, Zhang W, Yang W, Xu J, Lai J (2014) Rheological properties, morphology, mechanical properties, electrical resistivity and EMI SE of cyclic butylene terephthalate/graphite/carbon black composites. J Polym Res 21. https://doi.org/10.1007/s10965-014-0556-7

14. Chen Y, Chen Q, Lv Y, Huang Y, Yang Q, Liao X, Niu Y (2015) Rheological behaviors and electrical conductivity of long-chain branched polypropylene/carbon black composites with different methods. J Polym Res:22. https://doi.org/10.1007/s10965-015-0751-1

15. Motaung TE, Saladino ML, Luyt AS, Martino DC (2013) Influence of the modification, induced by zirconia nanoparticles, on the structure and properties of polycarbonate. Eur Polym J 49:2022–2030. https://doi.org/10.1016/j.eurpolymj.2013.04.019

16. Carrión FJ, Sanes J, Bermúdez MD (2007) Effect of ionic liquid on the structure and tribological properties of polycarbonate-zinc oxide nanodispersion. Mater Lett 61:4531–4535. https://doi.org/10.1016/j.matlet.2007.02.044

17. Luyt AS, Messori M, Fabbri P, Mofokeng JP, Taurino R, Zanasi T, Pilati F (2011) Polycarbonate reinforced with silica nanoparticles. Polym Bull 66:991–1004. https://doi.org/10.1007/s00289-010-0408-5

18. Ikeshima D, Nishimori F, Yonezu A (2019) Deformation modeling of polyamide 6 and the effect of water content using molecular dynamics simulation. J Polym Res 26. https://doi.org/10.1007/s10965-019-1815-4

19. Yi Y, Bi P, Zhao X, Wang L (2018) Molecular dynamics simulation of diffusion of hydrogen and its isotopic molecule in polystyrene. J Polym Res 25:1–6. https://doi.org/10.1007/s10965-017-1406-1

20. Sahputra IH, Echtermeyer AT (2014) Molecular dynamics simulations of strain-controlled fatigue behaviour of amorphous polyethylene. J Polym Res:21. https://doi.org/10.1007/s10965-014-0577-2

21. Vao-soongnern V, Merat K, Horpibulsuk S (2016) Interaction of the calcium ion with poly(acrylic acid) as investigated by a combination of molecular dynamics simulation and X-ray absorption spectroscopy. J Polym Res 23:1–7. https://doi.org/10.1007/s10965-015-0895-z

22. Sharifi S, Yazdani A, Rahimi K (2020) Effect of Co2+ content on supercapacitance properties of hydrothermally synthesized nanoparticles. Mater Sci Semicond Process 108:104902

23. Khoei AR, Khorrami MS (2016) Mechanical properties of graphene oxide: a molecular dynamics study. Fullerenes Nanotub Carbon Nanostructures 24:113–121. https://doi.org/10.1080/1536383X.2016.1208180

24. Mo Y, Zhang H, Xu J (2014) Molecular dynamic simulation of the mechanical properties of PI / SiO 2 nanocomposite based on materials studio. J Chem Pharm Res 6:1534–1539

25. Fermeglia M, Pricl S (2007) Multiscale modeling for polymer systems of industrial interest. Prog Org Coatings 58:187–199. https://doi.org/10.1016/j.porgcoat.2006.08.028

26. Resta V, Quarta G, Lomascolo M, Maruccio L, Calcagnile L (2015) Raman and photoluminescence spectroscopy of polycarbonate matrices irradiated with different energy 28Si+ ions. Vacuum 116:82–89. https://doi.org/10.1016/j.vacuum.2015.03.005

27. Lee S, Stolarski V, Letton A, Laane J (2000) Studies of bisphenol-a – polycarbonate aging by Raman difference spectroscopy. J Mol Struct 521:19–23

28. Debus J, Dunker D (2012) Raman studies on a heavily distorted polycarbonate sample - Raman-Untersuchungen an einer stark deformierten Polycarbonat-probe. Cond-mat.Mtrl-sci

29. Dybal J, Schmidt P, Baldrian J, Kratochvı J (1998) Ordered Structures in Polycarbonate Studied by Infrared and Raman Spectroscopy, Wide-Angle X-ray Scattering , and Differential Scanning Calorimetry. Macromolecules 9297:6611–6619

30. Kaur J, Shah J, Kotnala RK, Verma KC (2012) Raman spectra, photoluminescence and ferromagnetism of pure, co and Fe doped SnO2nanoparticles. Ceram Int 38:5563–5570. https://doi.org/10.1016/j.ceramint.2012.03.075

31. Pawlyta M, Rouzaud J-N, Duber S (2015) Raman microspectroscopy characterization of carbon blacks: spectral analysis and structural information. Carbon N Y 84:479–490. https://doi.org/10.1016/j.carbon.2014.12.030

32. Philipp HR, Legrand DG, Cole HS, Liu YS (1987) The optical properties of bisphenol-a polycarbonate. Polym Eng Sci 27:1148–1155. https://doi.org/10.1002/pen.760271507

33. Mark JE (2009) Polymer data hand book